MICRO-GENERATOR DESIGN FOR SMART GRID SYSTEM (COMPARATIVE STUDY)

*Adel El Shahat[1], Ali Keyhani[1] and Hamed El Shewy[2]
Department of Electrical and Computer Engineering, Ohio State University, USA[1]
Department of Electrical Power and Machines Engineering, Zagazig University, Egypt[2]
*Emails: adel.elshahat@ieee.org, ahmed.210@osu.edu

Abstract*—High Speed PM Generators driven by micro-turbines are widely used in Smart Grid System. So, this paper proposes comparative study among six classical, optimized and genetic analytical design cases for 400 kW output power at tip speed 200 m/s. These six design trials of High Speed Permanent Magnet Synchronous Generators (HSPMSGs) are: Classical Sizing; Unconstrained optimization for total losses and its minimization; Constrained optimized total mass with bounded constraints are introduced in the problem formulation. Then a genetic algorithm is formulated for obtaining maximum efficiency and minimizing machine size. In the second genetic problem formulation, we attempt to obtain minimum mass, the machine sizing that is constrained by the non-linear constraint function of machine losses. Finally, an optimum torque per ampere genetic sizing is predicted. All results are simulated with MATLAB, Optimization Toolbox and its Genetic Algorithm. Finally, six design examples comparisons are introduced with study of machines waveforms, THD and rotor losses.

Index terms*:* High Speed, Micro-Turbines, Optimization, PM Generators, Smart Grid, MATLAB.

I. INTRODUCTION

The Smart Grid Energy Systems (SGES) is recently increasing, particularly onsite generation [1]. This interest is because larger power plants are economically unfeasible in many regions due to increasing system and fuel costs, and more strict environmental regulations. In addition, recent technological advances in small generators, Power Electronics, Smart Metering, Mechatronics and energy storage devices have provided a new opportunity for distributed energy resources at the distribution level [1-3], [44-47]. So, more attention has been paid to the development of high speed PM generators driven by micro-turbines, as prime movers with local conversion at load

points [4]. High speed permanent magnet (PM) generators provide a substantial reduction in size and weight over other types of generators, and they are also higher in power density, since, as the speed of a machine increases, its size decreases for a given output power. Size, weight, and cost are the major factors for successful design. For high-speed applications, the rotor aspect ratio, defined as length-to-diameter, is a critical parameter. Stator core losses may be minimized by using laminated steel in stator construction and by not generating frequencies that are too high. The main applications of PMSG are for power generation as part of renewable energy resources and main generators for aircraft, etc. [5-12]. The sizing of HSPMSG design must address system topology for good power/volume, low cost, and superior efficiency. The influence of the choice of stator lamination material on iron loss in a high speed, high power, and permanent magnet generator is investigated. We study the optimum design of high speed PM alternators for applications in distributed power generation systems [4-17]. The high speed PM machine has been widely used in distributed power generation. The high speed generator distributed generation system, in comparison with the PM doubly-fed reluctance generator, for the same application, has better electromagnetic properties, and (the PM doubly-fed reluctance machine exhibits better mechanical behavior [25]. Aspects of PM motor technology and the design of brushless PM machines, as introduced in Hanselmann [15] and Hendershot [16], are used in this paper.

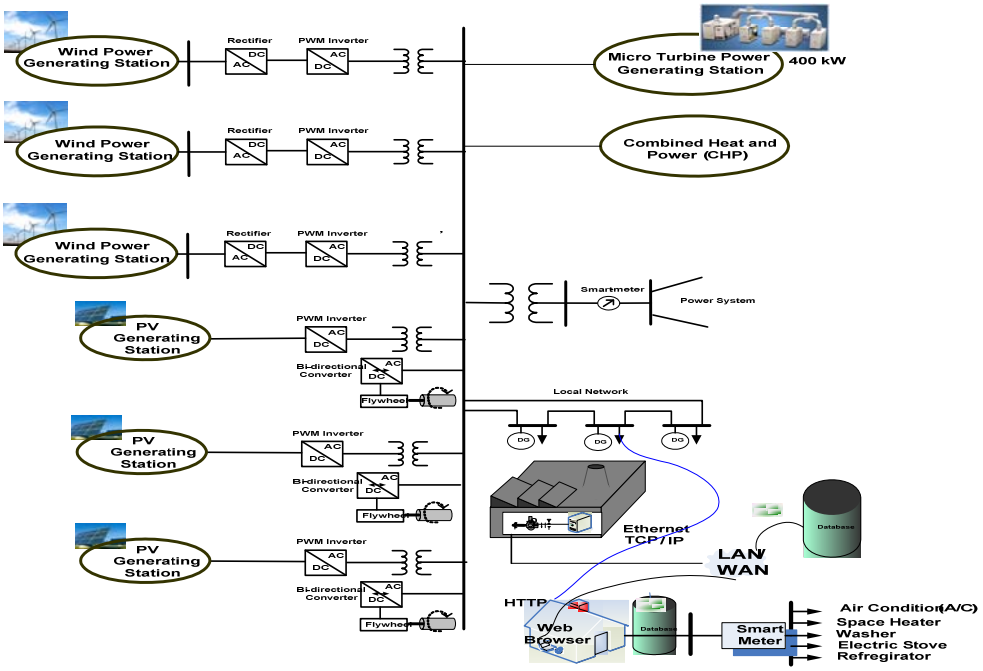

Figure 1. Smart Grid System with Micro Turbine Power Station [1]

II. MACHINE DESIGN PARAMETERS

A. Machine Materials

The rare earth magnets, SmCo and NdFeB, have become popular because of their greater power density, high Coercivity, high flux densities, and the linearity of their demagnetization curves [16] and [18]. NdFeB is preferred because it is cheaper and more readily available. Therefore, NdFeB magnets are selected for use in PMG, with some conservatively assumed values [17]. The rotor is usually built from the same material as the stator for ease of construction, but it can be made of any economical steel, provided it is strong enough for its function [16], [19]. TM19, 29 gauge electrical silicon steel is selected for the PMG because it is economical, its thin laminations minimize power losses due to the circulating eddy current, and because it has a saturation flux density of about 1.8 T [16], [17].

B. Mechanical Design

The stator is an important part of the machine because it serves as the main structural component, it provides the housing for the armature windings, and it completes the flux path for the magnetic circuit. Slotted stators are the traditional stator design and consist of openings around the stator for the armature windings. In this paper, the slots are trapezoidal, but assumed to be approximately rectangular. They contain form-wound windings so that the depression width is the same as the top slot width. Slotting is used because of its advantages, such as the achievement of a narrow air gap length to maximize the flux linkage, the increase in surface contact area between the windings, and a path of low thermal resistance, provided by stator steel for good heat conduction [17]. The initial design of the generator assumes a three-phase machine. Also, a 36 slots machine is chosen for the initial generator design [16]. A general machine mechanical shape is shown in figure 2.

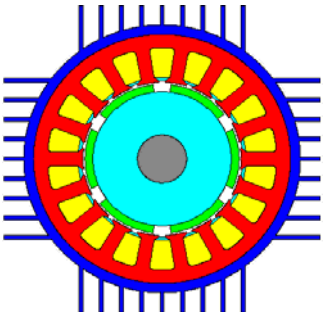

Figure 2. Surface mounted PM machine shape

The surface mounted permanent magnets in the rotor as shown in fig. 2 are selected here due to its suitability for high speed applications. For high-speed applications, the rotor aspect ratio, defined as length-to-diameter (L/D), is a critical parameter. PM machines offer flexibility in selecting pole sizes, which allows for smaller diameters. A normal L/D ratio for a wound rotor machine is 0.5 – 1.0, compared to 1 – 3 for a PM machine [20]. So, here it is selected to be 2.5. The rotor radius and rotational speed also determine the tip speed of the machine, which is the surface velocity of the rotor.

$$v_{tip} = r\omega_m \tag{1}$$

Where ω_m: angular speed (rad/sec); r: rotor radius (m)

C. Number of Poles and Magnets Pole Design

An even number of poles is always used, here P = 3, because this provides a balanced rotational design. Assuming a constant mechanical rotation speed, electrical frequency is given as.

$$N(2P) = 120\, f \tag{2}$$

Where N = speed (rpm); P = pole pairs; f = electrical frequency

If a PM generator is going to be the source of DC bus through a rectifier system, a high pole number is desirable because as the electrical frequency increases, support components such as filter capacitors and inductors can be much smaller. Therefore, for a given rotational speed, one cheap and efficient solution is to have a higher number of pole pairs and frequency. However, as the frequency increases, higher stator losses result because core losses are proportional to frequency squared. In addition, as the pole number gets larger, the number of slots per pole per phase decreases and can cause the voltage waveforms to become less sinusoidal so all factors must be considered. The pole arc of the magnets can also be varied. Magnets seldom span the full pole pitch because the flux at the transition between north and south poles leaks between poles without linking the coils in the stator. The gaps between the poles usually contain non – magnet pieces, such as soft iron, so that no flux crosses over the air gap between magnets. All full pole arc is $\square_{me}$ = 180 ^{o}E and produces a full voltage waveform but has increased harmonic content. As the pole arc is reduced (up to 20 – 30 %) and those areas are filled in with soft – iron pieces, the resulting flux waveform is more sinusoidal and has fewer harmonics and therefore lower rotor losses. The magnet poles are sometimes skewed to reduce cogging torque and smooth out variations in air gap reluctance, flux, and voltage waveforms. Skewing of magnets occurs axially

along the length of the rotor to provide a constant rotational torque and prevent pole pieces from exactly lining up with stator teeth. Magnet poles skew factor is selected to reduce cogging torque and smooth out variations in air gap reluctance, flux, and voltage waveforms.

$$k_{sn} = \frac{\sin(n\theta_s)}{\frac{\theta_s}{2}} \tag{3}$$

Where θs: Skew angle, rad E; n: Harmonic number

D. Magnetic Dimensions

The magnetic dimensions that affect a PM machine are air gap and magnet height. The air gap flux density (B_g) can be represented by Eq. 4. The radial air gap is made as small as possible to maximize the air gap flux density, minimize the flux leakage, and to produce a lower reluctance value.

$$B_g = \frac{h_m}{h_m + g} B_r \tag{4}$$

where h_m: Magnet height (mm); g: Air gap (mm); B_r: Magnet Remnant Flux Density (T)
Magnets losses are reduced, using smaller magnets. For uniform magnetic fields, the magnet height is usually larger than the air gap, by a factor 5 – 10.

E. Slots per Pole, Per Phase

Three-phase machines are typically used in this paper as the standard choice for most motors and generators. Another important design parameter is the number of slots per pole, per phase (m), as in Eq. 5.

$$m = \frac{N_s}{2 * P * q} \tag{5}$$

Varying the number of slots/pole/phase is used to produce a more sinusoidal voltage waveform and reduce machine harmonics.

F. Stator Windings

The pitch of a winding (α) refers to the angular displacement between the sides of a coil. The breadth of a stator winding results from the coils occupying a distribution of slots within a phase belt. In smaller machines, coils are composed of round insulated wires that are placed in the stator slot, along with insulation material. A slot fill factor (λ_s) is used to determine how much of the slot's cross-sectional area is occupied by winding material, as in Eq. 6.

$$\lambda_s = \frac{Winding \quad Area}{Total \quad Slot \quad Area} \tag{6}$$

Typically, machines contain two coils sides per slot, making the winding a double-layer design [16]. Overall, slot fill factors vary in value from 0.3 – 0.7, depending on the number and size of the conductors in the slots, as well as the amount of labor utilized. In this paper, a slot fill factor of 0.5 is assumed. Almost all machines use series, wye – connected windings because they provide the safest alternative. Therefore, wye series connected windings are selected for use in the designs in this study.

G. Machine Calculated Parameters

Each phase of the machine is modeled, as shown in Fig. 3.

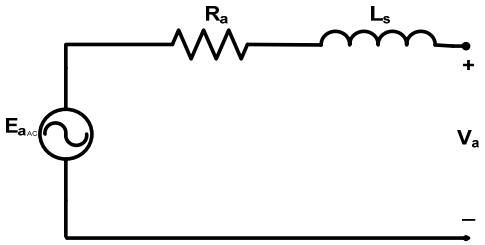

Figure 3. A Per Phase electrical model

Where: R_a: Armature resistance; L_s: Synchronous inductance; E_a: Back e.m.f voltage and V_a: Terminal voltage.

H. Winding Resistances

Resistance of copper phase windings is calculated in Eq. 7

$$R_a = \frac{l}{\sigma * A_{ac}} \tag{7}$$

Where l: length of conductor; σ : winding conductivity; A_{ac}: winding cross – sectional area

$$A_{ac} = \frac{A_s * \lambda_s}{2 * N_C} \tag{8}$$

Where A_s: slot Area, N_c: turns per coil

But the above stator resistance equation may be used as in low frequencies applications, so it has to be developed. Since the machine rotates at high speed, and high frequency and so the skin depth may be affected. In conductors that carry high frequency currents, skin effect can become an issue and affect the operation of the machine. Skin effect is caused by eddy currents in the windings themselves due to the changing magnetic field. These eddy currents force the current

flowing in the conductor to crowd to the outer edges of the conductor. This in turn causes the current to flow through a smaller cross – sectional area and increase the resistance of the conductor. It is well known that, when conductive material is exposed to an ac magnetic field, eddy currents are induced in the material in accordance with Lenz's law. The power loss resulting from eddy currents which can be induced in the slot conductors appears as an increased resistance in the winding. To understand this phenomenon, let us consider a rectangular conductor as shown in fig. 4. The average eddy current loss in the conductor due to a sinusoidal magnetic field in the y direction is given approximately by Hanselman [15].

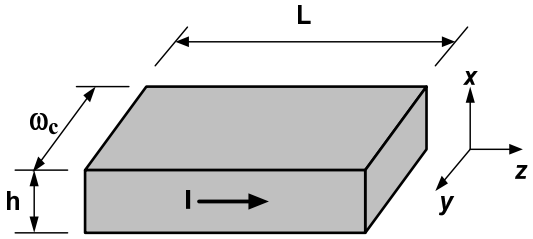

Figure 4. Rectangular conductor geometry

$$P_{ec} = \frac{1}{12}\sigma L\,\omega_c h^3 \omega^2 u_0^2 H_m^2 \tag{9}$$

Where H_m: the turn field intensity value; u_0: permeability of free space.

Since skin depth is defined as

$$\delta = \sqrt{\frac{2}{\omega u_0 \sigma}} \tag{10}$$

Equation (9) can be written as

$$P_{ec} = \frac{L\,\omega_c h^3}{6\sigma\delta^4} H_m^2 \tag{11}$$

Using this expression it is possible to compute the ac resistance of the slot conductors. If the slot conductors are distributed uniformly in the slot, and substituting the field intensity into eq. (11) and summing over all ns conductors gives a total slot eddy current loss of

$$P_e = \left(\frac{d_s L h^2 n_s^2}{9\sigma\delta^4 \omega_s}\right) I^2 \tag{12}$$

Where I is the rms conductor current; ω_s: Slot width(m); d_s: Slot depth(m)

The slot resistance of a single slot containing ns conductors connected in series is

$$R_{sl} = \frac{\rho n_s^2 L}{k_{cp}\,\omega_s d_s} \tag{13}$$

Where L: the slot length; k_{cp}: the conductor packing factor, is the ratio of cross sectional area occupied by conductors to the entire slot area and ρ: electrical resistivity (Ω.m).

Using eq. (13), the total slot resistance can be written as

$$R_{st} = R_{sl} + R_{ec} = R_{sl}(1 + \Delta_e) \tag{14}$$

In this equation, $\Delta e = R_{ec}/R_{sl}$ is the frequency-dependent term. Using eq. (13) and eq. (12), this term simplifies to

$$\Delta_e \equiv \frac{R_{ec}}{R_{sl}} = \frac{1}{9}\left(\frac{d_s}{\delta}\right)^2 \left(\frac{h}{\delta}\right)^2 \tag{15}$$

This result shows that the resistance increases not only as a function of the ratio of the conductor height to the skin depth but also as a function of the slot depth to the skin depth. Thus, to minimize ac losses, it is desirable to minimize the slot depth as well as the conductor dimension. For a fixed slot cross-sectional area, this implies that a wide but shallow slot is best.

I. Winding and Magnet Factors

Winding are short-pitched and have breadth associated with them. To account for these effects, a winding factor (kw) is utilized, as in Equation 16.

$$k_{wn} = k_{pn} * k_{bn} \tag{16}$$

Short-pitching is an important means for eliminating harmonics and improving the power quality of the machine. The pitch factor is shown in Equation 17.

$$k_{pn} = \sin\left(\frac{n * \alpha}{2}\right) * \sin\left(\frac{n * \pi}{2}\right) \tag{17}$$

The breadth factor explains the effect of the windings occupying a distribution or range of slots within a phase belt. The breadth factor is derived in Equation 18.

$$k_{bn} = \frac{\sin\left(\frac{n * m * \gamma}{2}\right)}{m * \sin\left(\frac{n * \gamma}{2}\right)} \tag{18}$$

Where m: slots per pole per phase; γ: coil electrical angle

The magnetic flux factor equation [15], for the slotted stator and surface magnet configuration is shown in Equation 19.

$$k_{gn} = \frac{R_i^{np-1}}{R_s^{2np} - R_i^{2np}} * [(\frac{np}{np+1}) * (R_2^{np+1} - R_1^{np+1}) + \frac{np}{np-1} * R_s^{2np} * (R_1^{1-np} - R_2^{1-np})] \quad (19)$$

Where R_s: outer magnetic boundary, R_2: outer boundary of magnet; R_i: inner magnetic boundary, R_1: inner boundary of magnet

J. Flux and Voltage

For useful voltage, only the fundamental components are used to determine the internal voltage (back e.m.f) of the generator, as shown in Equations 20, 21, and 22.

$$E_a = \omega_0 \lambda \quad (20)$$

$$\lambda = \frac{2 * R_s * L_{st} * N_a * k_w * k_s * B_1}{P} \quad (21)$$

$$B_1 = \frac{4}{\pi} * B_g * k_g * \sin(\frac{P\theta_m}{2}) \quad (22)$$

Where θ_m: magnet physical angle

$$B_g = \frac{k_l C_\phi}{1 + k_r * \frac{u_{rec}}{PC}} * B_r \quad (23)$$

Where u_{rec}: recoil permeability; B_r: remnant flux density

$$PC = \frac{h_m}{g_e * C_\phi} \quad (24)$$

Where PC: permeance coefficient; C_Φ: flux concentration factor (Am/Ag)

$$N_a = 2 * P * N_c \quad (25)$$

Where N_c : Turns per coil; N_a : Number of armature turns (each slot has 2 half coils)

$$\tau_s = w_s + w_t; g_e = k_c * g \quad (26)$$

Where g_e: eff. air gap; w_s: average slot width; w_t: tooth width

Here, a leakage factor (Kl ≅ 0.95) and a reluctance factor (Kr ≅1.05) are both used for surface magnets. The presence of the slots in the stator also affects the air gap flux density because of the difference in permeance caused by the slots. Carter's coefficient (k_c) is used to account for this effect [15].

$$k_c = [1 - \frac{1}{\frac{\tau_s}{w_s} * (5 * \frac{g}{w_s} + 1)}]^{-1} \tag{27}$$

The terminal voltage (V_a) is calculated from the internal voltage (E_a), and the synchronous reactance voltage drop. The armature resistance is usually ignored because it is much smaller than synchronous reactance. The voltage is found as a relation in output power (P_{wr}), e.m.f, and reactance from the resulting quadratic equation.

$$V_a = \sqrt{\frac{-BB + \sqrt{BB^2 - 4CC}}{2}} \tag{28}$$

$$BB = \frac{2}{3} X_s P_{wr} - E_a^2 \; ; \quad CC = \frac{2}{9} X_s^2 P_{wr}^2$$

K. Machine Inductances

In a slotted PM machine, there are three distinct components of inductance: the largest, air gap inductance slot leakage inductance, and the smallest, end-turn inductance. The total inductance for the phase is the sum of the three inductances, ignoring other small factors.

$$L_s = L_{ag} + L_{slot} + L_e; \quad X_s = \omega_0 * L_s \tag{29}$$

The air gap inductance is given by Eq. 30.

$$L_{ag} = \frac{\lambda}{i} = \frac{q}{2} * \frac{4}{n\pi} * \frac{u_0 * R_s * L_{st} * N_a^2 * k_{wn}^2}{n^2 * P^2 * (g + h_m)} \tag{30}$$

The slot leakage inductance is presented in Eq. 31. Assume the slot is rectangular with slot depressions, as in Fig. 2, and assume (m) slots per pole per phase, with a standard double layer winding.

$$L_{slot} = L_{as} - L_{am}; (3\,phase) \tag{31}$$

$$L_{am} = 2 * P * L_{st} * Perm * N_{sp} * N_c^2 \tag{32}$$

$$L_{as} = 2*P*L_{st}*Perm*[4*N_c^2(m - N_{sp}) + 2*N_{sp}*N_c^2] \tag{33}$$

A slot permeance per unit length is shown in Equation 34.

$$Perm = \frac{1}{3} * \frac{h_s}{w_{st}} + \frac{h_d}{w_d} \tag{34}$$

The end turn inductance is introduced in Eq. 35, assuming the end turns are semi-circular, with a radius equal to one-half the mean coil pitch.

$$L_e = \frac{u_0 * N_c * N_a{}^2 * \tau_s}{2} * \ln\left(\frac{\tau_s * \pi}{\sqrt{2 * A_s}}\right) \tag{35}$$

L. Basic Losses

Losses in a machine consist of core losses, conductor losses, friction and windage losses, and rotor losses. Rotor losses will be discussed later. Stator core losses, per weight, can be greater than normal in machines because of higher frequencies. These losses are minimized by using laminated steel in stator construction and by not generating frequencies that are too high. Core losses consist of hysteresis and eddy current losses. The best way to approximate core losses is to use empirical loss data. An exponential curve fitting is applied to the empirical data for M-19, 29 gauge material, in order to obtain an equation for estimating core losses, as in Equation 36, with constant values in [22].

$$P_C = P_0 * \left(\frac{B}{B_0}\right)^{\varepsilon B} * \left(\frac{f}{f_0}\right)^{\varepsilon f} \tag{36}$$

Where P_0: Base power; B_0: Base flux density; ε_B: Flux density exponent; f_0: Base frequency; ε_f: Frequency exponent

The above commonly used equation considering hysteresis and eddy-current loss is not completely satisfactory, because the measured iron loss is much higher than theoretically calculated. This is so because it assumes a homogenous magnetization of the laminations, which is not a valid representation of what happens during the magnetization process. The loss caused by the movements of the magnetic domain walls is higher than the loss calculated with the commonly used equation. The difference between measured and calculated loss is called the excess loss or the anomalous loss. Sometimes, this anomalous or excess loss is considered as a third contribution to the iron loss. Great efforts have been made to calculate this excess loss, because of the complexity of the domain patterns. For reasons mentioned before, it is useful to represent the core loss by core loss resistance, which is placed in equivalent circuit. The core loss resistance is connected across the voltage V_a. Therefore, the power dissipated in this resistance is [26-34].

$$P_{R_c}(\omega) = \frac{V_a^2}{R_c} \tag{37}$$

$$R_c(\omega) = \frac{3\pi^2 L_{st}{}^2 N_a^2 \sqrt{\omega}}{8 c_{Fe} k_{Fe} (\frac{1}{\omega_0})^{1.5} (\frac{1}{B_0})^2 \{m_{st} (\frac{p\beta_{slot}}{b_{st}})^2 + m_{sy} (\frac{1}{h_{sy}})^2\}} \tag{38}$$

Where R_c: core resistance, c_{Fe}: correction factor for iron loss calculation, b_{st}: stator tooth width, k_{Fe}: specific iron loss, m_{st}: stator teeth mass, βslot: slot angle, h_{sy}: stator yoke height

When this core loss resistance is depicted in an equivalent circuit, it should be noted that the resistance is frequency dependent.

The conductor losses are found, using Equation 39.

$$P_a = q * I_a^2 * R_a \tag{39}$$

For rotors operating at high speed, the friction and windage in air can cause losses which result in inefficiency and heat production. These losses are calculated, using the power necessary to overcome the drag resistance of a rotating cylinder, as given by Eq. 40 [23].

$$P_{wind} = C_f * \pi * \rho_{air} * \omega^3 * R^4 * L_{st} \tag{40}$$

The coefficient of friction can be approximated by Eq. 41.

$$C_f \cong 0.0725 * R_{ey}^{-0.20} \tag{41}$$

Where R_{ey}: Reynold's Number

III. CLASSICAL SIZING

For the basic sizing calculations, an air-cooled generator is assumed with 10 psi [16], [24]. The machine power equation is utilized to derive the rotor radius and stack length of the machine, as in Equation 42.

$$P_{wr} = 2 * \pi * r * L_{st} * v_{tip} * \tau \tag{42}$$

Where r : rotor radius; L_{st} : stack length; τ : shear stress (psi)

The L/D ratio is substituted for L_{st}. Using shear stress, rotor tip speed, and machine power rating range, the power equation is calculated to obtain rotor radius and stack length, while matching the desired rotational speed of the machine with a L/D ratio equal to 2.5, as supposed here. Using a pole pair value of 3, a slot height of 10 mm, and a slot fill fraction of 0.5, the frequency is found.

Once the basic sizing of the machine is complete, in-depth analysis is conducted to obtain the overall performance. Using the equations presented in previous sections, all the detailed parameters can be obtained. The lengths, volumes, masses, and overall generator parameters are calculated, using basic geometric equations and relationships. A 15% service mass fraction is added to the total mass estimate to account for the additional services associated with machines cooling [17], [24]. Once the mass of each of the stator parts is known, core losses are estimated in accordance with them. The calculation of lengths, volumes, and weights are presented. The mass of armature conductors, core mass, magnet mass, and shaft mass are calculated to give the total mass value. Finally, stator resistance, terminal voltage, current, loss types, input power, and efficiency are calculated.

IV. ANALYTICAL MODEL

This part presents the study of rotor losses caused by stator winding time and space harmonics slot space harmonics.

A. Rotational Stress and Retaining Sleeve

Since the PM generator is spinning at high speed, the rotor and permanent magnets are subjected to extremely high centrifugal forces. These forces can cause significant amounts of damage if the magnets and rotor are not properly restrained. The rotational components can be strengthened by enclosing them in a retaining sleeve/can which also increases the air gap length. The centrifugal force on the magnets due to the rotor spinning is calculated in Eq. (43)

$$F_{cen} = \frac{M_m . v_{mag}^2}{R + h_m} \tag{43}$$

Where M_m: mass of magnets; v_{mag}: velocity of magnets

Using the inner surface area of the retaining sleeve, this force is converted to an outward pressure. Treating the retaining sleeve as a thin-walled vessel, the loop stress felt by the sleeve is determined as shown in Eq. (44)

$$\sum_{vert} F_v = -2.\sigma_c .h.L + \int_0^{\pi} P.r.L.\sin(\theta).L.d\theta = 0$$
$$\sigma_C = \frac{P.r}{h} \tag{44}$$

A suitable safety factor is applied to the hoop stress to get a final SF stress for the retaining sleeve. The retaining sleeve can be made from many different types of materials including metal alloys and composites. A disadvantage of a metallic sleeve is eddy currents are induced in the sleeve by variations in the flux density caused by the stator slots [40 – 42]. From our calculations with various materials with our initial gap length; it is not sufficient once the retaining sleeve is considered (since the air gap dimension includes the retaining sleeve thickness). So, the machine must therefore be revised to allow for the retaining can and redesigned taking the retaining sleeve and hoop stress limits into consideration. But, this updated machine will be bigger one with a much larger air gap, greater magnet height, lower B_g, lower voltage, and higher current density. So, we prefer her not to use the sleeve and keep the smaller machine with restriction to the manufacturer to firm the magnet rigidly.

B. Rotor Losses

1) Model for Time Harmonics & Winding Space Harmonics

The permanent magnets used in high-speed generators are electrically conductive and therefore support eddy currents. The retaining sleeves are sometimes made from electrically conductive material that also can carry eddy currents. These eddy currents are primarily caused by fluctuations in the magnetic flux density produced by time and space harmonics of the winding currents. The currents produce losses which can potentially cause excessive heating or demagnetization of the permanent magnets. An analytical model is developed using the winding and current harmonics and the surface impedance to estimate the rotor losses. Fig. 5 shows the PM generator geometry “flattened out” into rectilinear coordinates. This is an accurate representation provided the dimensions are on a radial scale that is much smaller than the radius of the machine so that curvature is not important [40-42]. The direction of rotation is in the positive x-direction, the radial direction is y, and the armature current flows in the axial dimension, z.

The following assumptions are made in developing the rotor analytical loss model:

- Layers of material extend to ± infinity in the ± x direction.
- Layers effectively extend to negative infinity in the negative y direction.
- Motion/rotation is in the + x direction.
- The physical constants of the layers are homogeneous, isentropic, and linear.

- The ferromagnetic material does not saturate.
- The machine is long axially so magnetic variations in the z direction are ignored (H and B only vary in x, y directions).
- All currents flow in the z direction.
- The rotor and stator are constructed of laminated steel so their conductivity in the z direction is negligible.
- The time and space variations are approximately sinusoidal.
- Flux density at y = infinity is zero.
- A traveling flux wave harmonic can be represented by an equivalent current sheet (K_z) on the surface of the stator.
- The normal component of the flux density is continuous at all interfaces.
- The tangential component of the flux density is continuous at all interfaces except at the stator/air gap where it is increased by the current sheet density.
- The magnetic flux density crossing the air gap and the magnets is perpendicular.
- The effect of magnet eddy currents on the magnetic flux density is negligible – this is accurate below 10 kHz [43].
- The magnet flux density is constant over the magnet breadth

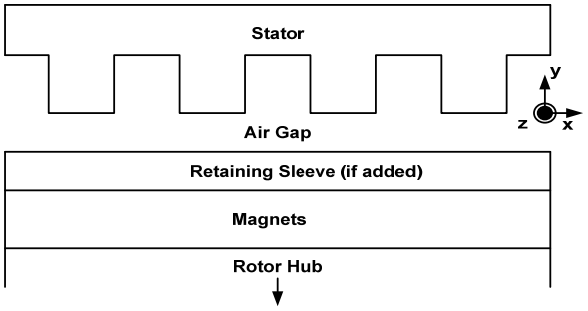

Figure 5. General Magnet Loss Model

$$-<S_y>=-\frac{1}{2}\left|k_z\right|^2.\mathrm{Re}(Z_s)$$

$$-<S_y>=-\frac{1}{2}\left|H_x\right|^2.\mathrm{Re}(\frac{E_z}{H_x}) \tag{45}$$

$$-<S_y>=-\frac{1}{2}\mathrm{Re}(E_z.\bar{H}_x)$$

Eq. (45) yields the power dissipated at the stator surface. This is the correct result for the rotor because there is no mechanism for dissipating power between the stator and rotor. The power estimated by Poynting's theorem flows directly from the stator to the rotor [42].

$$z_s = \frac{\omega_n}{k_n}.u_0.\sigma \tag{46}$$

$$z_s = \frac{E_{surf}}{k_{surf}} = \frac{E_z}{-H_x} = \frac{\frac{-\omega_n}{k_n}.u_0.H_y}{-H_x}$$

Surface impedance (Z_s) is the ratio of the z-directed electric field to the z-directed current, Eq. (46). A final expression for the top surface coefficient is determined Eq. (47), and it is applicable to any uniform region.

$$\alpha_t = j.\frac{k}{\gamma}.[\frac{j.\frac{k}{\gamma}.\sinh(\gamma h) + \alpha_b.\cosh(\gamma h)}{j.\frac{k}{\gamma}.\cosh(\gamma h) + \alpha_b.\sinh(\gamma h)}] \tag{47}$$

If the region being examined is positioned on top of a ferromagnetic surface, such as the magnets on the steel rotor shaft, the boundary condition at the bottom of the layer ($\alpha b \to \infty$ as $Hx \to 0$) produces Eq. (48).

$$\alpha_t = j.\frac{k}{\gamma}.\coth(\gamma h) \tag{48}$$

In the case of the air gap where the conductivity is zero, Eq. (47) reduces to Eq. (49).

$$\alpha_t = j.[\frac{j.\sinh(\gamma h) + \alpha_b.\cosh(\gamma h)}{j.\cosh(\gamma h) + \alpha_b.\sinh(\gamma h)}] \tag{49}$$

At the top of the layer (y=h), the surface coefficient is shown in Eq. (50).

$$\alpha_t = j.\frac{k}{\gamma}.(\frac{\frac{H_p}{H_n}.e^{\gamma h} - .e^{-\gamma h}}{\frac{H_p}{H_n}.e^{\gamma h} + .e^{-\gamma h}}) \tag{50}$$

A surface coefficient is defined as the ratio of the y-directed to x-directed magnetic field amplitude (α = HY/HX). At the bottom of the layer where y = 0, the surface coefficient is given by Eq. (51).

$$\alpha_b = j.\frac{k}{\gamma}.\left(\frac{\frac{H_p}{H_n} - 1}{\frac{H_p}{H_n} + 1}\right) \tag{51}$$

$$H_x = \mathrm{Re}[H_X.e^{j.(\omega t - kx)}] \tag{52}$$

$$H_y = \mathrm{Re}[H_Y.e^{j.(\omega t - kx)}]$$

Solving for the magnetic flux densities and magnetic fields produces Eq. (52), also all these analyses are done with the aid of Faraday's Law, Maxwell's Law and Ampere Law. In order to calculate the rotor losses, the above analytical model is applied to the geometry in fig. 5. For this model, the stator is assumed to be a smooth surface without slots because the slot effects are consider later. The first step is calculating the surface coefficient at the bottom of the magnet layer. It is assumed that this is formed by the highly permeable rotor shaft below the magnets. This assumption allows the surface coefficient at the top of the magnet layer to be calculated also.

2) Model for Stator Slot Effects

The stator slots cause variations in the magnetic field which losses in the retaining sleeve and magnets of the rotor. Accurate calculation of the losses in the retaining sleeve is extremely difficult. Several different methods have been developed and in this paper, the technique from reference [16] is employed. As the rotor spins past the slot openings of the stator, the air gap flux density undergoes modulation due to the change in reluctance. The dip in B_g (shown in fig. 6) travels along the B-waveform which is otherwise moving synchronously with the rotor.

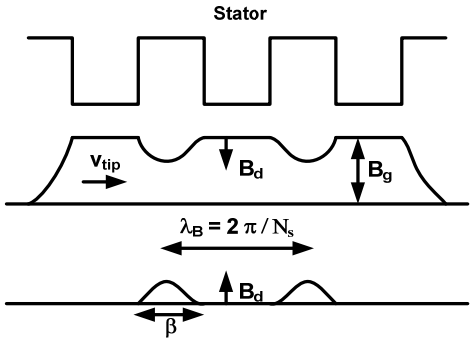

Figure 6. Flux Density Variation

The rotation of the rotor generates an E-field in the sleeve and a subsequent axial current density J=E/p. When this current density is integrated over the volume of the can, the average loss per unit area is determined Eq. (53) [16].

$$w = \frac{\pi^2}{3600} \cdot \frac{[B.N.(R+hm)]^2.t}{\rho} \qquad (53)$$

$$B = \frac{B_d}{\sqrt{2}} \cdot \sqrt{\frac{\beta}{\lambda_B}}$$

It is evident from Eq. (53) that as the slot width increases, the width of the flux density dip (β) gets larger causing the sleeve losses to increase. The above equation only considers eddy currents flowing in the axial direction but there are also circumferential components. These portions are accounted for using a factor K_s as shown in Eq. (54) where the total can losses are determined [16].

$$P_{can} = K_s.w.A \qquad (54)$$

$$A = \pi.2.(R+h_m).L_{st}$$

$$K_s = 1 - \frac{\tanh[\frac{\rho.L_{st}}{2.(R+h_m)}]}{[\frac{\rho.L_{st}}{2.(R+h_m)}]}$$

One way to reduce the retaining losses is to split the sleeve cylinder (if used) into separate rings. The magnet losses are calculated using methods similar to Eq. (53) and Eq. (54) assuming that the eddy current flow in the top 10% of the magnet volume.

3) Machine THD

HSPM generator produces back EMF waveforms that are dependent on a number of factors as discussed before. The goal is to produce a voltage waveform that closely resembles a sinusoidal waveform with a low total harmonics distortion (THD) because this results in minimal harmonic content which reduces losses in the machine. THD is a measure of the distortion in a waveform caused by undesirable frequency components. It is calculated as shown in Eq. (55).

$$THD = \sqrt{\frac{\sum_{(n\neq 1)} E_{anrms}^2}{E_{a1rms}^2}} \qquad (55)$$

The back EMF waveforms are generated using the below eq.s

$$B(\theta) = \sum_{\substack{n=1 \\ n\_odd}}^{\infty} B_n.\sin(np\theta)$$

$$B_n = \frac{4}{n\pi}.B_g.k_{gn}.\sin(\frac{np\theta_m}{2}).\sin(\frac{n\pi}{2}) \quad (56)$$

θ_m: magnet physical angle; n: harmonic number

$$\lambda(\theta) = \sum_{\substack{n=1 \\ n\_odd}}^{\infty} \lambda_n.\sin(np\theta)$$

$$\lambda_n = \frac{2.R_s.L_{st}.N_a.B_n.k_{wn}.k_{sn}}{p} \quad (57)$$

$$Ea = \sum_{\substack{n=1 \\ n\_odd}}^{\infty} v_n.\sin(np\theta)$$

$$v_n = \frac{d}{dt}\lambda_n = \omega_0\lambda_n \quad (58)$$

V. CLASSICAL SIZING RESULTS

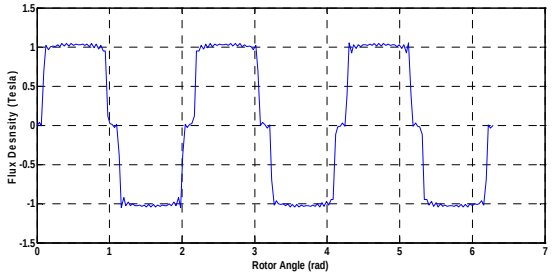

Figure 7. Initial Flux Density Waveform

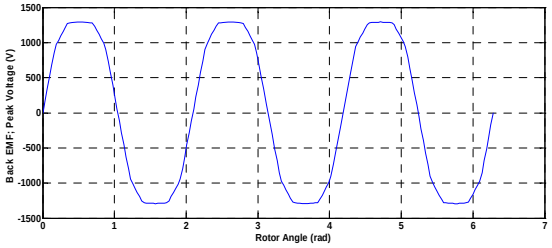

Figure 8. Initial EMF Waveform

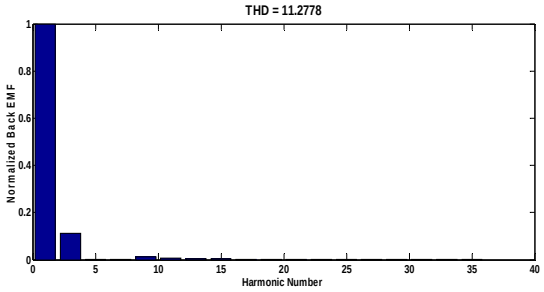

Figure 9. Initial Harmonic Content (11.2778 %) for case 1

VI. UNCONSTRAINED NON-LINEAR OPTIMIZATION

Unconstrained minimization entails finding a vector, x, that is a local minimum of a scalar function, f (x), without restriction.

A. Trust-Region Methods

To understand the trust-region approach to optimization, we consider the unconstrained minimization problem to minimize f (x). Suppose we are at a point, x, in n-space and we want to improve its position. The basic idea is to approximate f with a simpler function, q, which reasonably reflects the behavior of function f in a neighborhood, N, around point, x. This neighborhood is the trust region. A trial step, s, is computed by minimizing over N. This is the trust-region sub-problem, min s {q(s), s ∈ N} [35]. The current point is updated to be x + s, if f (x + s) < f (x); otherwise, the current point remains unchanged and N, the region of trust, is shrunk and the trial step computation is repeated. The key questions in defining a specific trust-region approach to minimizing f(x) are how to choose and compute the approximation, q, (defined at the current point, x,), how to choose and modify the trust-region, N, and how to accurately solve the trust-region sub-problem. In the standard trust-region method, the quadratic approximation, q, is defined by the first two terms of the Taylor approximation, to F at x; the neighborhood, N, is usually spherical or ellipsoidal in shape. Mathematically, the trust-region sub-problem is typically stated as

$$\min\{\frac{1}{2}s^T Hs + s^T g \_ such \_ that \left\|Ds\right\| \le \Delta \tag{59}$$

Where g is the gradient of f at the current point, x, H is the Hessian matrix (the symmetric matrix of second derivatives), D is a diagonal scaling matrix, Δ is a positive scalar, and $\|\cdot\|$ is the 2-norm.

Good algorithms exist for solving the previous equation; such algorithms typically involve the computation of a full Eigen system and a Newton process applied to the secular equation [35].

$$\frac{1}{\Delta} - \frac{1}{\|s\|} = 0 \tag{60}$$

Such algorithms provide an accurate solution to the equation. However, they require time, proportional to several factorizations of H.

B. Fminsearch Algorithm

Fminsearch uses the Nelder-Mead simplex algorithm, as described in [36]. This algorithm uses a simplex of n + 1 points for n-dimensional vectors, x. The algorithm first makes a simplex around the initial guess, x0, by adding 5% of each component, x0(i) to x0, and using these n vectors as elements of the simplex, in addition to x0. (It uses 0.00025 as component i, if x0(i) = 0.) Then the algorithm modifies the simplex repeatedly, according to the following procedure.

1. Let x(i) denote the list of points in the current simplex, i = 1,...,n+1.

2. Order the points in the simplex from the lowest function value f(x(1)) to the highest f(x(n+1)). At each step in the iteration, the current worst point, x(n+1), is discarded, and another point is accepted into the simplex (or, in the case of Step 7 below, all n points with values above f(x(1)) are changed).

3. Generate the reflected point r = 2m – x(n+1), where m = Σx(i)/n, i = 1...n, and calculate f(r).

4. If f(x(1)) ≤ f(r) < f(x(n)), accept r and terminate this iteration. Reflect.

5. If f(r) < f(x(1)), calculate the expansion point, s, s = m + 2(m – x(n+1)), and calculate f(s).

a. If f(s) < f(r), accept s and terminate the iteration. Expand.

b. Otherwise, accept r and terminate the iteration. Reflect.

6. If f(r) ≥ f(x(n)), perform a contraction between m and the better of x(n+1) and r:

a. If f(r) < f(x(n+1)) (i.e., r is better than x(n+1)), calculate c = m + (r – m)/2 and calculate f(c). If f(c) < f(r), accept c and terminate the iteration. Contract outside. Otherwise, continue with Step 7. (Shrink.)

b. If f(r) ≥ f(x(n+1)), calculate cc = m + (x(n+1) – m)/2 and calculate f(cc).

If f(cc) < f(x(n+1)), accept cc and terminate the iteration. Contract inside. Otherwise, continue with Step 7. (Shrink.)

7. Calculate the n points v(i) = x(1) + (x(i) – x(1))/2 and calculate f(v(i)), i = 2,...,n+1. The simplex at the next iteration is x(1), v(2),...,v(n+1). Shrink.

C. *Total Losses Minimization Sizing*

Using the previous technique minimizes total losses. The first step is to choose the optimizing variables, x1, x2, and x3; these variables here are the L/D ratio, the Rotor radius, and Stack length, respectively. The second step is to formulate the total losses function to be minimized as fitness or objective function. The third step, using optimization tool box GUI with a proper choice for initial variables values.

$$P_{Total\_Losses} = P_{Core} + P_{Conductor} + P_{Wind} \tag{61}$$

The L/D ratio (x1) is substituted for Lst (x2) with a pole pair value of 3, a slot height of 10 mm, 36 slots and a slot fill fraction of 0.5, the power factor is considered as 0.999999 ≈ 1.

D. *Results*

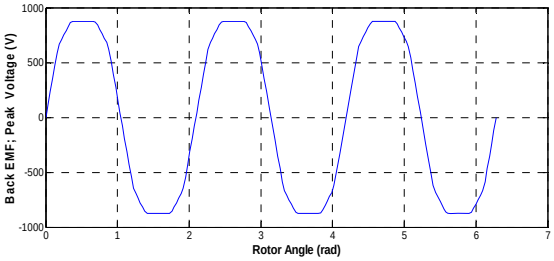

Figure 10. Initial Flux Density Waveform

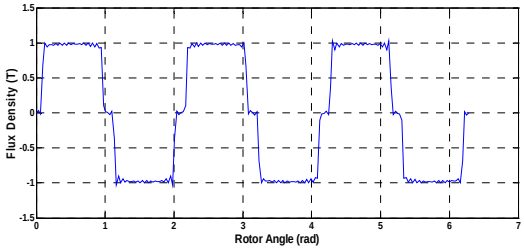

Figure 11. Initial EMF Waveform

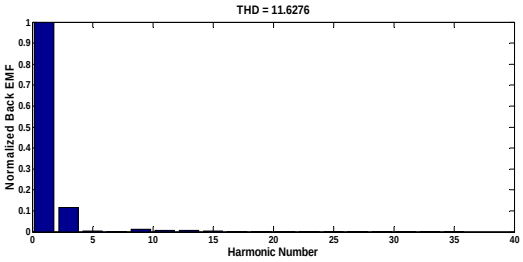

Figure 12. Initial Harmonic Content (11.6276 %) for case 2

VII. SIMPLE CONSTRAINED OPTIMIZATION

When trying to use unconstrained optimization in this case, from the beginning, the maximum value for the L/D ratio exceeds its upper limit. Constraints are used as bounds from 0.0 to 3.0. The function used here is presented as follows.

A. fmincon Active Set Algorithm

In constrained optimization, the general aim is to transform a problem into an easier sub-problem that can then be solved and used as the basis of an iterative process. A characteristic of a large class of early methods is the translation of the constrained problem into a basic unconstrained problem, by using a penalty function for constraints that are near or beyond the constraint boundary. By this means, the constrained problem is solved using a sequence of parameterized unconstrained optimizations, which in the limit will cover the constrained problem. These methods are now considered relatively inefficient and have been replaced by methods that focused on the solution of the Karush-Kuhn-Tucker (KKT) equations. The KKT equations are necessary conditions for optimality in a constrained optimization problem. If the problem is a so-called convex programming problem, that is, one in which f(x) and Gi(x), i = 1,...,m, are convex functions, then the KKT equations are both necessary and sufficient for a global solution point. The Kuhn-Tucker equations can be stated as

$$\begin{aligned} &\nabla f(x^*) + \sum_{i=1}^{m} \lambda_i . \nabla G_i(x^*) = 0 \\ &\lambda_i . G_i(x^*) = 0, i = 1, ..., m_e \\ &\lambda_i \geq 0, i = m_e + 1, ..., m, \end{aligned} \tag{62}$$

The first equation describes a canceling of the gradients between the objective function and the active constraints at the solution point. For the gradients to be canceled, Lagrange multipliers (λi, i = 1,...,m) are necessary to balance the deviations in the magnitude of the objective function and constraint gradients. Because only active constraints are included in this canceling operation, constraints that are not active must not be included in this operation and, so, are given Lagrange multipliers equal to 0. This is stated implicitly in the last two Kuhn-Tucker equations. The solution of the KKT equations forms the basis for many nonlinear programming algorithms. These algorithms attempt to compute the Lagrange multipliers, directly. Constrained quasi-Newton methods guarantee super-linear convergence by accumulating second-order information regarding the KKT equations using a quasi-Newton updating procedure. These methods are

commonly referred to as Sequential Quadratic Programming (SQP) methods, since a QP sub-problem is solved at each major iteration. These are known as Iterative Quadratic Programming, Recursive Quadratic Programming, and Constrained Variable Metric methods. The 'active-set' algorithm is not a large-scale algorithm.

B. Large-Scale vs. Medium-Scale Algorithms

An optimization algorithm is large-scale when it uses linear algebra that does not need to store, nor operates on, full matrices. This algorithm may be done internally by storing sparse matrices and by using sparse linear algebra for computations, whenever possible. Furthermore, internal algorithms either preserve sparsity, such as in a sparse Cholesky decomposition, or they do not generate matrices, such as those generated in a conjugate gradient method. Large-scale algorithms are accessed by setting the Large Scale option to the "On" position, or by setting the Algorithm option appropriately; this is solver-dependent. In contrast, medium-scale methods internally create full matrices and use dense linear algebra. If a problem is sufficiently large, full matrices take up a significant amount of memory, and dense linear algebra may require a long time to execute. Medium-scale algorithms are accessed by setting the Large Scale option to the "Off" position, or by setting the Algorithm option appropriately; this is solver-dependent. Don't let the term "large-scale" mislead you; you can use a large-scale algorithm on a small problem. Furthermore, you do not need to specify any sparse matrices to use a large-scale algorithm. Choose a medium-scale algorithm to access extra functionality, to possibly improve performance, such as that by additional constraint types.

C. Total Mass Minimization Sizing

We use the previous technique with the function described above to minimize total mass. The optimizing variables, x1, x2, and x3, are the same. We then formulate the total mass function to be minimized as a fitness function in the form of a Matlab m – file. (Later, using optimization tool box GUI with a proper choice for initial variables values. Also, it should be noted that the large-scale trust-region method does not currently solve this type of problem, but that using a medium scale (line search) does. The desired optimization function here is illustrated in Equation (63); each part of the equation is a function of the optimizing variables.

$$M_{Total} = M_{Core} + M_{Magnet} + M_{Shaft} + M_{Conductor} + M_{Service} \tag{63}$$

$$M_{core} = M_{cb} + M_{ct} \tag{64}$$

$$M_{cb} = \rho_s \pi (R_{co}^2 - R_{ci}^2) L_{st} \quad (65)$$

Where M_{cb}: back iron mass (kg); : steel density (kg/m3); R_{co}: core outside radius; R_{ci}: core inside radius

$$R_{ci} = R + h_m + g + h_d + h_s \quad (66)$$

Where h_m: Magnet thickness(m); g: air gap (m); h_d: slot depression depth(m); h_s: slot depth (m)

$$R_{co}=R_{ci}+dc \quad (67)$$

Where dc: stator core back iron depth (m)

$$M_{ct} = \rho_s L_{st} (N_s w_t h_s + 2 \pi R h_d - N_s h_d w_d) \quad (68)$$

Where M_{ct}: teeth mass; N_s: number of slots; w_t: tooth width; w_d: slot depression width(m)

$$M_{Magnet} = 0.5 (p \theta_m ((R + h_m)^2 - R^2) L_{st} \rho_m \quad (69)$$

Where θ_m: Magnet physical angle(rad); ρ_m: Magnet density; p: pole pairs number

$$M_{Shaft} = \pi R^2 L_{st} \rho_s \quad (70)$$

$$M_{Conductor} = 3 L_{ac} A_{ac} \rho_c \quad (71)$$

Where L_{ac}: armature conductor length; A_{ac}: armature conductor area (assumes form wound); ρ_c: conductor density

$$L_{ac} = 2 N_a (L_{st} + 2 l_{e2}) \quad (72)$$

$$A_{ac} = A_s \lambda_s / (2 N_c) \quad (73)$$

Where N_a: number of armature turns; l_{e2}: end length (half coil); A_s: slot area; λ_s: slot fill fraction; N_c: turns per coil

A 15% service mass fraction is added to the total mass estimate to account for the additional services associated with machines cooling [37].

$$M_{Service} = 0.15 (M_{Conductor} + M_{Shaft} + M_{Magnet} + M_{Conductor}) \quad (74)$$

D. Results

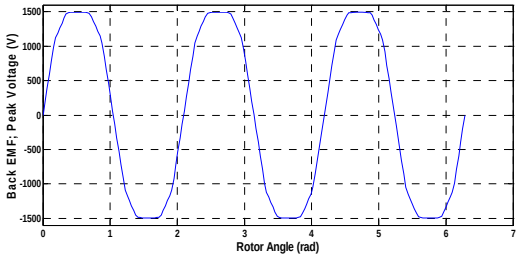

Figure 13. Initial Flux Density Waveform

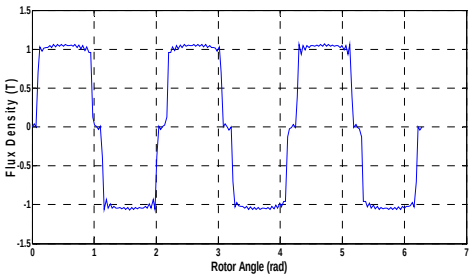

Figure 14. Initial EMF Waveform

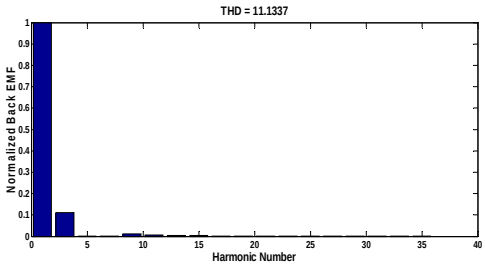

Figure 15. Initial Harmonic Content (11.1337 %) for case 3

VIII. GENETIC ALGORITHM HSPMSG SIZING

The genetic algorithm is a method, based on the idea of natural selection, the process that drives biological evolution, which is used here in solving both constrained and unconstrained optimization problems. At each stage of development, the genetic algorithm selects “individuals,” at random, from the current “population” to be “parents,” and uses them to produce the “children” of the next generation. In this way, the genetic algorithm repeatedly modifies a population of individual solutions. Over successive generations, the population "evolves" towards an optimal solution. We can apply the genetic algorithm to solve a variety of optimization problems that are not well-suited for standard optimization algorithms, including problems in which the objective function is discontinuous, non-differential, stochastic, or highly nonlinear.

A. Description of the Non-Linear Constraint Solver

The genetic algorithm uses the Augmented Lagrangian Genetic Algorithm (ALGA) to solve non-linear constraint problems. The optimization problem solved by the ALGA algorithm is min x f (x), such that

$$c_i(x) \leq 0,\ i = 1 \ldots m;$$
$$c_{eqi}(x) = 0,\ i = m+1 \ldots m_t \quad (75)$$

$$A \cdot x \leq b;\ A_{eq} \cdot x = b_{eq}$$
$$lb \leq x \leq ub,$$

Where c (x) represents the non-linear inequality constraints, c_{eq} (x) represents the equality constraints, m is the number of non-linear inequality constraints, and m_t is the total number of non-linear constraints.

The Augmented Lagrangian Genetic Algorithm (ALGA) attempts to solve a non-linear optimization problem with non-linear constraints, linear constraints, and bounds. In this approach, bounds and linear constraints are handled separately from non-linear constraints. A sub-problem is formulated by combining the fitness function and non-linear constraint function, using the Lagrangian and the penalty parameters. A sequence of such optimization problems are approximately minimized, using the genetic algorithm, such that the linear constraints and bounds are satisfied. A sub - problem formulation is defined as

$$\Theta(x,\lambda,s,\rho) = f(x) - \sum_{i=1}^{m} \lambda_i s_i \log(s_i - c_i(x)) + \sum_{i=m+1}^{mt} \lambda_i c_i(x) + \frac{\rho}{2} \sum_{i=m+1}^{mt} c_i(x)^2 \tag{76}$$

Where the components λ_i of the vector (λ) are nonnegative and are known as Lagrange multiplier estimates. The elements s_i of the vector (s) are non – negative shifts, and ρ is the positive penalty parameter.

The genetic algorithm minimizes a sequence of the sub-problem, which is an approximation of the original problem. When the sub-problem is minimized to a required accuracy and satisfies feasibility conditions, the Lagrangian estimates are updated. Otherwise, the penalty parameter is increased by a penalty factor. This results in a new sub-problem formulation and minimization problem. These steps are repeated until the stopping criteria are met. For a complete description of the algorithm, see [38] and [39].

B. Efficiency Maximizer Genetic Sizing

The optimization variables here are the same; that is, x1, x2, and x3 are the L/D ratio, the rotor radius, and the rotor stack length, respectively. The efficiency function is implemented in the form of m. file. (After that, using the genetic algorithm, with the previous technique, to maximize the function and generate the desired variables for this maximization (or by more accurate word by optimizing this function with a simple constraints that are [1 0 0] as lower limit, and [3 1 1] as upper limit. Using these optimizing variables, we can deliver all the detailed variables for the desired HSPMSG, at maximum efficiency. Also, it is important to adjust all options in the

Genetic GUI in a proper manner, especially the mutation function, population, selection, and stopping criteria.

$$\eta = \frac{P_{out}}{P_{input}} \tag{77}$$

$$P_{input} = P_{Total\_Losses} + P_{out} \tag{78}$$

C. Results

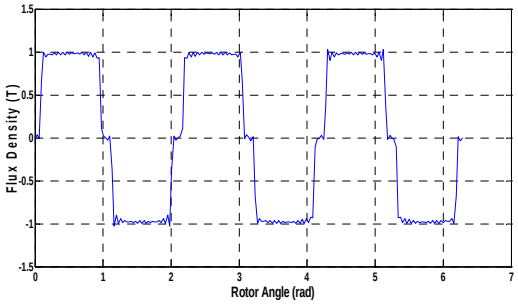

Figure 16. Initial Flux Density Waveform

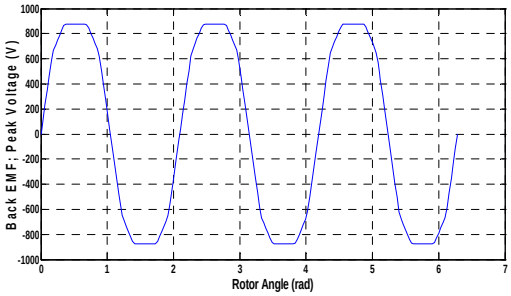

Figure 17. Initial EMF Waveform

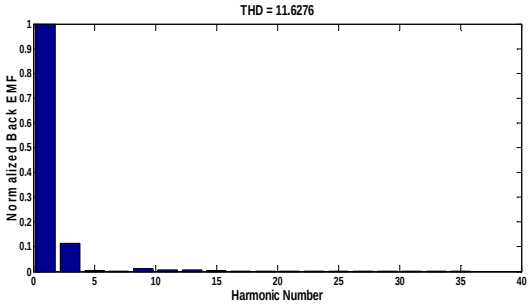

Figure 18. Initial Harmonic Content (11.6276 %) for case 4

IX. MINIMUM MASS GENETIC SIZING, CONSTRAINED BY MINIMUM LOSS

We will take one case from the previous examples, using the total mass function (m.file) as a fitness function in GA. The same optimizing variables and the same bounds as used in the first genetic example, also using non-linear constraint function with the aid of minimum loss value obtained from the part of Min. Loss. The non-linear constraint function, which governs the optimization process, is implemented using the minimum losses value at the same values of tip speed and power

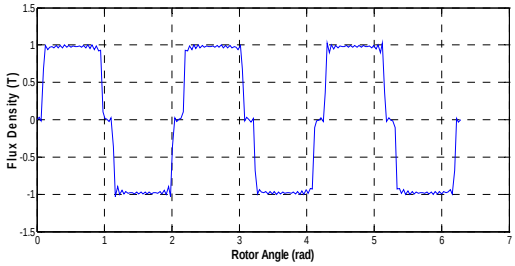

Figure 19. Initial Flux Density Waveform

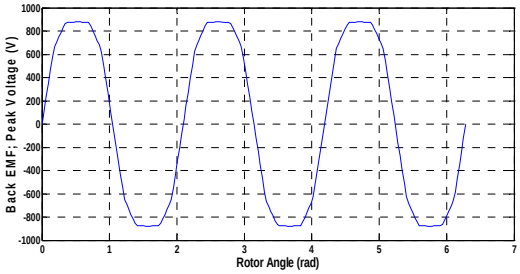

Figure 20. Initial EMF Waveform

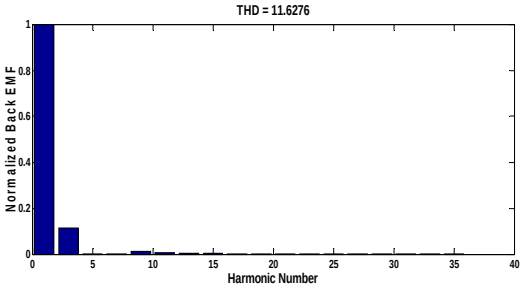

Figure 21. Initial Harmonic Content (11.6276 %) for case 5

X. OPTIMUM TORQUE PER AMPERE GENETIC SIZING

Optimum torque per ampere control is considered one of the best PM synchronous machine control strategies. So, as a new idea or question arises, why can't we design for optimum torque per ampere HSPMSM with, the aid of the genetic algorithm? This trial investigates this idea. The optimization variables here are the same; that is, x1, x2, and x3 are the L/D ratio, the rotor radius, and the rotor stack length, respectively. (Then implement the optimum torque per ampere function as fitness function, in the form of m. file. After that, using the Genetic Algorithm, with the previous technique, to maximize the function and generate the desired variables for this maximization or by more accurate word by optimizing this function with a simple constraints that are [1 0 0] as lower limit, and [3 1 1] as upper limit. Using these variables, we can deliver the detailed variables for the desired HSPMG, at an optimum torque per ampere. Also, the main goal is to set all options in the Genetic GUI in a proper manner, especially mutation function one; also the population, selection, and stopping criteria, etc. must be adjusted. As in the design equations above, the torque per ampere could be presented as MTA = 3 Ea / ωe, ; this expression is used in the Matlab m.file function.

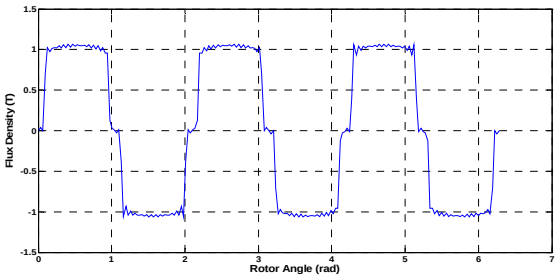

Figure 22. Initial Flux Density Waveform

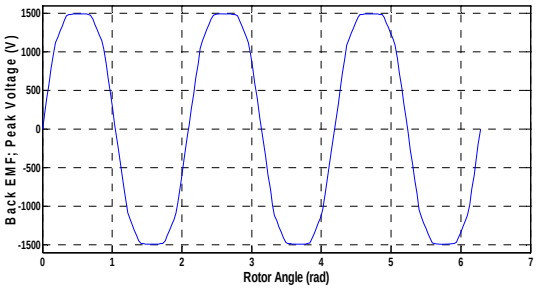

Figure 23. Initial EMF Waveform

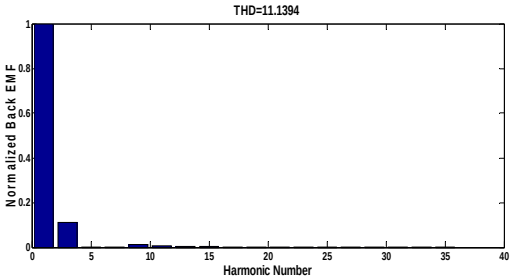

Figure 24. Initial Harmonic Content (11.1394 %) for case 6

XI. COMPARATIVE MODELS

The part introduces comparisons among the six cases which are: case 1; for classical sizing, case 2; Total Losses Minimization Sizing, Case 3; Total Mass Minimization Sizing, Case 4; Efficiency Maximizer Genetic Sizing, Case 5; Minimum Mass Genetic Sizing, Constrained by Minimum Losses, and case 6; Optimum Torque per Ampere Genetic Sizing. These examples are at tip speed = 200 m/s and output power = 400 Kw.

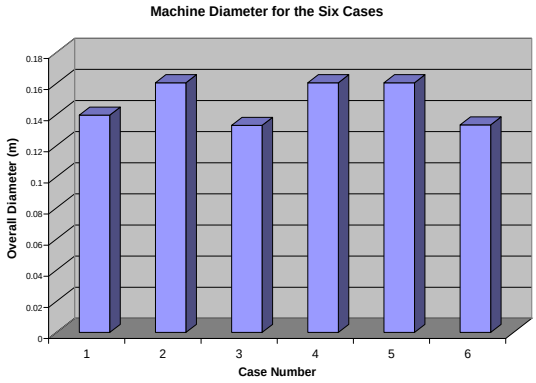

Figure 25. Overall Machine Diameter Comparisons

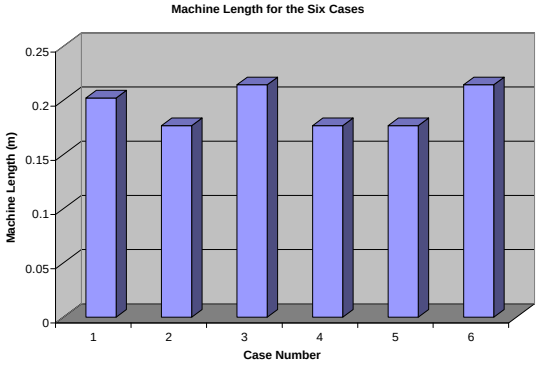

Figure 26. Overall Machine Length Comparisons

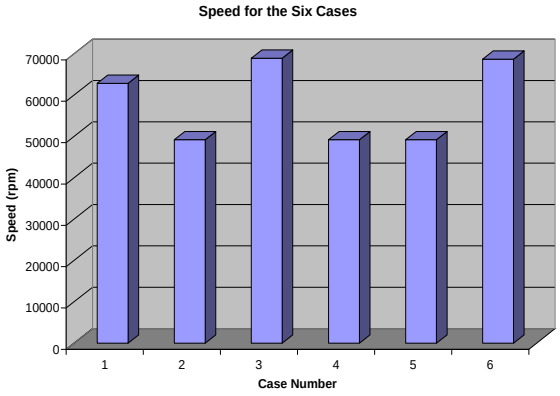

Figure 27. RPM Speed Comparisons

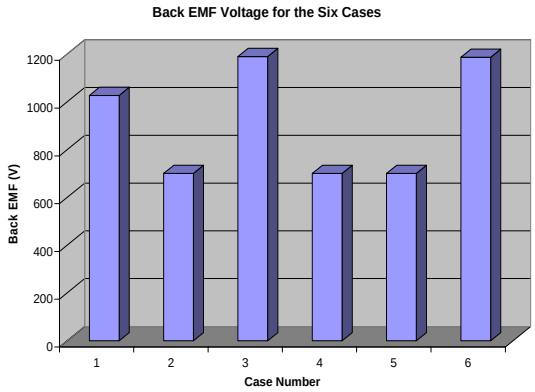

Figure 28. Back EMF Comparisons

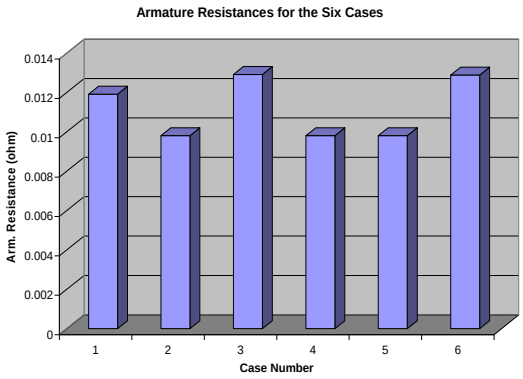

Figure 29. Armature Resistance Comparisons

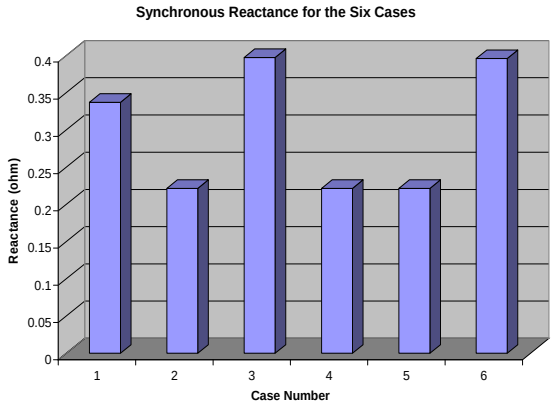

Figure 30. Synchronous Reactance Comparisons

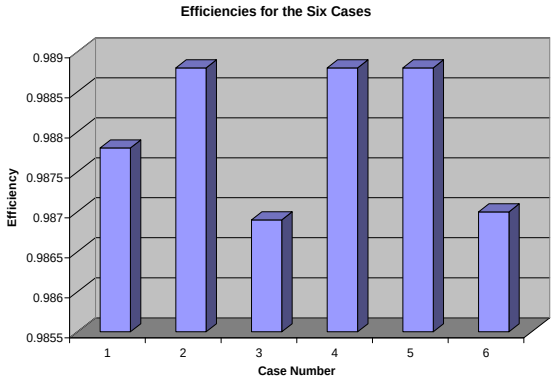

Figure 31. Efficiency Comparisons

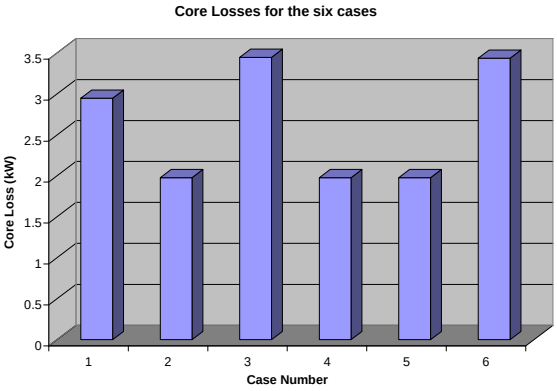

Figure 32. Core Loss Comparisons

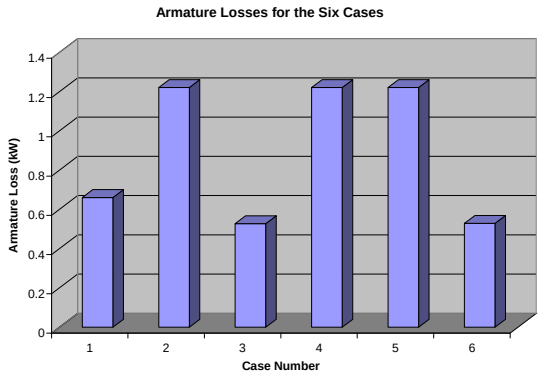

Figure 33. Armature Loss Comparisons

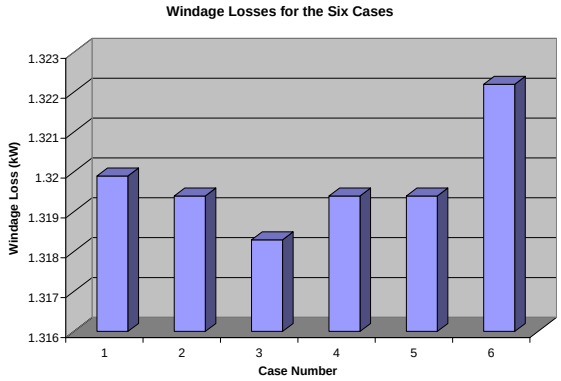

Figure 34. Windage Loss Comparisons

Figure 35. Total Mass Comparisons

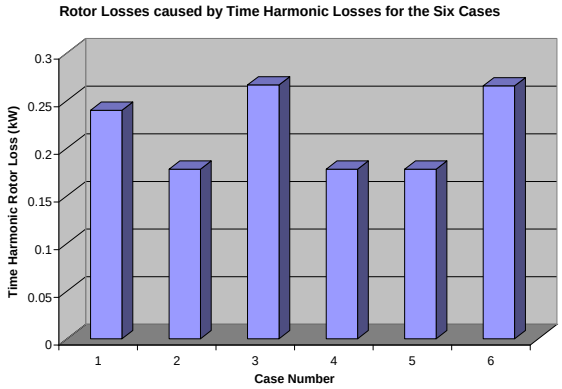

Figure 36. Rotor Loss Caused by Time Harmonics Comparisons

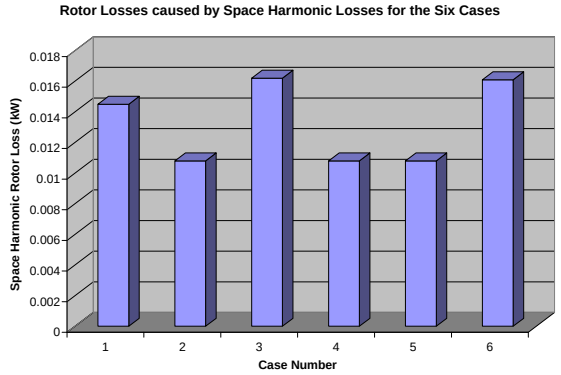

Figure 37. Rotor Loss Caused by Space Harmonics Comparisons

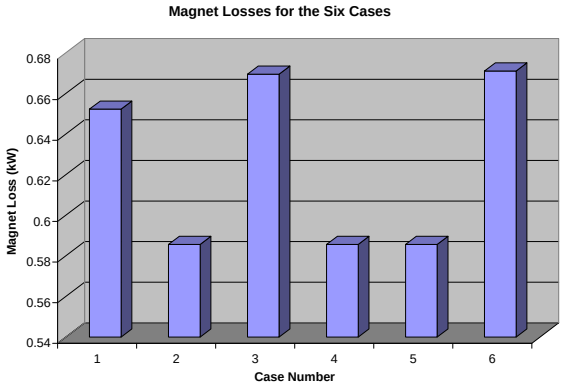

Figure 38. Magnet Loss Comparisons

XII. CONCLUSIONS

The sizing method presented gives a step by step method for high speed PM generator design. This paper illustrates the benefits of HSPM generators, compared to the original PM synchronous generators, since it offers significant reductions in both weights and volumes. It discusses the electrical and magnetic sizing of HSPMGs, at 400 kW power and tip speed of 400 m/s. Unconstrained optimization for the minimization of total loss is performed; this function of minimizing total losses is implemented and results are presented. The optimizing variables are rotor length to diameter ratio, rotor radius, and stack length, for each of the functions, in both constrained and unconstrained optimization and in the genetic algorithm. The constrained optimized total mass with some constraints is set up to keep the total mass to be minimized. It should be noted that the large-scale trust-region method does not currently solve this type of problem, but using medium scale line search has provided an acceptable performance. It was found that using the genetic algorithm in HSPMSG sizing will solve both constrained and unconstrained optimization problems. The results of the genetic algorithm are presented with the same optimization variables, as before, but the fitness functions, in which the constraints are varied for both efficiency maximization and genetic sizing. We also used the genetic algorithm to maximize efficiency. We have also presented minimum mass genetic sizing, constrained by minimum losses. The same optimizing variables and the same bounds are used in the genetic example, with non-linear constraint function of minimum losses. This is done under the condition of minimum total losses, equal to, or less than, the minimum total losses value. We have observed that this will have the benefit of limiting machines losses. In our study, we have found that a noticeable improvement appears in the performance parameters.

REFERENCES

[1] Ali Keyhani, Mohammad N. Marwali, and Min Dai, "Integration of Green and Renewable Energy in Electric Power Systems," Text Book, Wiley, January 2010

[2] Ali Keyhani, "Cyber-Controlled Smart Microgrid Systems of the Future: The High Penetration of Renewable and Green Energy Sources", New Research Directions for Future

Cyber-Physical Energy Systems Conference, Sheraton Baltimore City Center Hotel Baltimore, Maryland, pp. 1-3, June 2009

[3] Ali Keyhani, Jin-Woo Jung, Min Dai, "Control of Renewable Energy Sources in Smart Grid Systems," Smart Grids Africa Conference, pp. 1-13, 28-30 July 2008, Johannesburg, South Africa

[4] Ahmad, R. A., Pan, Z., and Saban, D. M., "On-Board Electrical Network Topology Using High Speed Permanent Magnet Generators," Electric Ship Technologies Symposium, 2007. ESTS apos;07. IEEE Volume , Issue , 21-23, pp.356 – 362, May 2007.

[5] Scridon, S., Boldea, I., Tutelea, Blaabjerg, L., F., and Ritchie, E., "BEGA – A Biaxial Excitation Generator for Automobiles: Comprehensive Characterization and Test Results," IAS, 2004, Industry Applications Conference, 2004. 39th IAS Annual Meeting Conference Record of the 2004 IEEE, vol.3, pp. 1682 – 1690, 3-7 Oct. 2004.

[6] Binder, A., Schneider, T., and Klohr, M., "Fixation of Buried and Surface- Mounted Magnets in High-Speed Permanent-Magnet Synchronous Machines," IEEE Trans. On Industry Applications, Vol. 42, NO. 4, pp. 1031 – 1037, July/August, 2006.

[7] Hosseini, S. M., Mirsalim, M. A., and Mirzaei, M. , "Design, Prototyping, and Analysis of a Low Cost Axial-Flux Coreless Permanent-Magnet Generator," IEEE Trans. On Magnet., Vol. 44, No. 1, pp. 75 – 80, Jan. 2008.

[8] Mellor, P.H., Burrow, S.G., Sawata, T., and Holme, M., "A Wide – Speed – Range Hybrid Variable – Reluctance / Permanent – Magnet Generator for Future Embedded Aircraft Generation Systems," IEEE Trans. On Industry Applications, Vol. 41, No. 2, pp. 551 – 556, March/April 2005.

[9] Sadeghierad, M., Lesani, H., Monsef, H., and Darabi, A., "Design considerations of High Speed Axial Flux permanent magnet Generator with Coreless Stator," The 8th International Power Engineering Conference (IPEC), pp. 1098 – 1102, 2007.

[10] Arnold, D. P., Das, S., Park, J. W., Zana, I., Lang, J. H., and Allen, M. G., "Micro fabricated High-Speed Axial-Flux Multi watt Permanent- Magnet Generators—Part II: Design, Fabrication, and Testing," Journal Of Micro Electromechanical Systems, Vol. 5, No. 5, pp. 1351 – 1363, October 2006.

[11] Paulides, J. J. H., Jewell, G. W., and Howe, D., "An Evaluation of Alternative Stator Lamination Materials for a High – Speed, 1.5 MW, Permanent Magnet Generator," IEEE Trans. On Magnetics, Vol. 40, No. 4, pp. 2041 - 2043, July 2004.

[12] Jang, S. M., Cho, H. W., and Jeong, Y. H., "Influence on the rectifiers of rotor losses in high – speed permanent magnet synchronous alternator," Journal of Applied Physics, 08R315, American Institute of Physics, 08R315-1 – 08R315-3, pp. 1-3, 2006.

[13] Kolondzovski, Z., "Determination of critical thermal operations for High – speed permanent magnet electrical machines," The International Journal for Computation and Mathematics in Electrical and Electronic Engineering, Vol. 27 No. 4, pp. 720-727, 2008.

[14] Nagorny, A. S., Dravid, N. V., Jansen, R. H., and Kenny, B. H., "Design Aspects of a High Speed Permanent Magnet Synchronous Motor / Generator for Flywheel Applications," NASA/TM—2005-213651 June 2005, International Electric Machines and Drives Conference sponsored by the IEEE Industry Applications Society, IEEE Power Electronics Society, IEEE Power Engineering Society, and IEEE Industrial Electronics Society, San Antonio, Texas, May 15–18, 2005.

[15] Hanselmann, D. C., Brushless Permanent Magnet Motor Design, Text Book, New York: McGraw-Hill, 1994.

[16] Hendershot, J. R. and Miller, T. J. E., Design of Brushless Permanent Magnet Motors, Text Book, Oxford, U.K.: Magna Physics Publishing and Clarendon Press, 1994.

[17] Rucker, J. E., Kirtley, J. L., McCoy, Jr. T. J., "Design and Analysis of a Permanent Magnet Generator For Naval Applications," IEEE Electric Ship Technologies Symposium, pp. 451 – 458, 2005.

[18] Kang, D., Curiac, P., Jung, Y., and Jung, S., "Prospects for magnetization of large PM rotors: conclusions from a development case study," IEEE trans. On Energy Conversion, vol. 18, no. 3, pp. 409-416, Sept. 2003.

[19] Paulides, J., Jewell, G., and Howe, D., "An evaluation of alternative stator lamination materials for a high speed, 1.5 MW, permanent Magnet Generator," IEEE Trans. On Magnetics, vol. 40, no. 4, pp. 2041-2043, July 2004.

[20] Bianchi, N., and Lorenzoni, A., "Permanent magnet generators for wind power industry: an overall comparison with traditional generators," Opportunities and advances in international power generation, conference publication No. 419, pp. 49-54, 1996.

[21] Rahman, M. A., and Slemon, G. R., "Promising Applications of Neodymium Iron Boron Iron Magnets in Electrical Machines," IEEE Trans. On Magnetics, Vol. No. 5, pp. 1712-1716, Sept 1985.

[22] Polinder, H. and Hoeijmakers, M. J., "Eddy – Current Losses in the Segmented Surface Mounted Magnets of a PM Machine," IEE Proceedings, Electrical Power Applications, Vol. 146, No. 3, pp. 261-266, May 1999.

[23] Aglen, O., and Andersson, A., "Thermal Analysis of a High Speed Generator," Industry Applications Conference, 38th IAS Annual Meeting. Con. vol.1, pp. 547- 554, 12-16 Oct. 2003. Current Version Published: 2004-01-07 IEEE Transactions, 2003.

[24] Pepi, J., and Mongeau, P., " High power density permanent magnet generators," Text Book, DRS Electric power technologies, Inc., 2004.

[25] Kong X., Wang F., and Sun Y. "Comparison of High Speed PM Generator with PM Doubly Fed Reluctance Generator for Distributed Power Generation System", 2nd IEEE Conference on Industrial Electronics and Applications, 2007. ICIEA 2007, pp. 1193 – 1197, 2007.

[26] I. Boldea and S. A. Nasar, Induction Machine Handbook, Text Book, CRC Press, Boca Raton, Fl, 2001.

[27] B. Amin, "Contribution to iron-loss evaluation in electrical machines", European Trans. on Elect. Power Eng., vol. 5, pp. 325-332, 1995.

[28] Z.Q. Zhu, D. Howe, E. Bolte, B. Ackermann, "Instantaneous Magnetic Field distribution in brushless permanent-magnet dc motors, part I: open-circuit field", IEEE Trans. on Magnetics, vol. 29, pp. 124-135, 1993.

[29] Z.Q. Zhu, D. Howe, "Instantaneous Magnetic Field distribution in brushless permanent-magnet dc motors, part II: armature-reaction field", IEEE Trans. on Magnetics, vol. 29, pp. 136-142, 1993.

[30] Z.Q. Zhu, D. Howe, "Instantaneous Magnetic Field distribution in brushless permanent-magnet dc motors, part III: effect of stator slotting", IEEE Trans. on Magnetics, vol. 29, pp. 143-151, 1993.

[31] Z.Q. Zhu, D. Howe, "Instantaneous Magnetic Field distribution in brushless permanent-magnet dc motors, part IV: magnetic field on load", IEEE Trans. on Magnetics, vol. 29, pp. 152-158, 1993.

[32] J.G. Zhu, S.Y.R. Hui, V.S. Ramsden, "Discrete modelling of magnetic cores including hysteresis, eddy current, and anomalous losses", IEE Proc., Part A, Sc., Measure. and Tech., vol. 140, pp. 317-322, 1993.

[33] I. Boldea, Variable speed electric generators, Text Book, CRC Press, Florida, 2006.

[34] J.G. Zhu, S.Y.R. Hui, V.S. Ramsden, "A generalized dynamic circuit model of magnetic cores for low- and high-frequency applications - Part I: Theoretical calculation of the equivalent core loss resistance", IEEE Trans. Power Elect., vol. 11, pp.246-250, 1996.

[35] Moré, J.J. and Sorensen D.C. "Computing a Trust Region Step", SIAM Journal on Scientific and Statistical Computing, Vol. 3, pp 553-572, 1983.

[36] Zhang, Y. "Solving Large-Scale Linear Programs by Interior-Point Methods Under the MATLAB Environment", Department of Mathematics and Statistics, University of Maryland, Baltimore County, Baltimore, MD, Technical Report TR96-01, 1995.

[37] Pepi, J. and Mongeau, P. , High power density permanent magnet generators, Text Book, DRS Electric power technologies, Inc, 2004.

[38] Conn, A. R., Gould N. I. M., and Toint Ph. L. "A Globally Convergent Augmented Lagrangian Algorithm for Optimization with General Constraints and Simple Bounds", SIAM Journal on Numerical Analysis, Volume 28, Number 2, pages 545–572, 1991.

[39] Conn, A. R., Gould N. I. M., and Toint Ph. L. "A Globally Convergent Augmented Lagrangian Barrier Algorithm for Optimization with General Inequality Constraints and Simple Bounds", Mathematics of Computation, Volume 66, Number 217, pages 261–288, 1997.

[40] I. H. Shames, and J. M. Pitarresi, Introduction to Solid Mechanics, Text Book, 3rd Ed., Prentice Hall, 2000.

[41] M. F. Ashby, and D. R. H. Jones, Engineering Materials, Text Book, Pergamon Press, 1991.

[42] J. L. Kirtley, and E. C. Lovelace, "Drag Loss in Retaining Rings of Permanent Magnet Motors," SatCon Technology Corporation, pp. Vol. 2, pp. 1068-1072, June 2003.

[43] H. Polinder and M. J. Hoeijmakers, "Eddy-Current Losses in the Permanent Magnets of a PM Machine," EMD 97, Conference Publication No. 444, pp. 138-142, 1997.

[44] A.Lay-Ekuakille, G. Vendramin, A. Fedele, L. Vasanelli, A. Trotta, "PV Maximum Power Point Tracking Through Pyranometric Sensor: Modelling and Characterization",

International Journal on Smart Sensing and Intelligent Systems, Vol. 1, No. 3, pp. 659-678, Sept. 2008

[45] Zhu Zhen, A. Al-Mamun and Myint Phone Naing, "Control-Centric Simulator for Mechatronics Design Case Study: Gyroscopically Stabilized Single Wheel Robot", International Journal on Smart Sensing and Intelligent Systems, Vol. 2, No. 2, pp. 190-199, June 2009.

[46] Shubhajit Roy Chowdhury, Dipankar Mukherjee, Hiranmay Saha, " FPGA Based Maximum Power Point Tracker of Partially Shaded Solar Photovoltaic Arrays using Modified Adaptive Perceptive Particle Swarm Optimization", International Journal on Smart Sensing and Intelligent Systems, Vol. 2, No. 4, pp.661-675, Dec. 2009.

[47] S.C.Mukhopadhyay, " Prediction of Thermal Condition of Cage-Rotor Induction Motors under Non-Standard Supply Systems", International Journal on Smart Sensing and Intelligent Systems, Vol. 2, No. 3, pp. 381-395, Sept. 2009